Revista ARACÊ
ISSN: 2358-2472

HYDROCLIMATIC CHANGES IN THE CAETÉ RIVER WATERSHED, EASTERN BRAZILIAN AMAZON

MUDANÇAS HIDROCLIMÁTICAS NA BACIA HIDROGRÁFICA DO RIO CAETÉ, AMAZÔNIA ORIENTAL BRASILEIRA

CAMBIOS HIDROCLIMÁTICOS EN LA CUENCA DEL RÍO CAETÉ, AMAZONÍA ORIENTAL BRASILEÑA

https://doi.org/10.56238/arev9n1-029

Submitted on: 01/05/2025 **Publication date:** 02/05/2026

Dênis José Cardoso Gomes[1], Norma Ely Santos Beltrão[2], Letícia Pereira da Silva[3]

ABSTRACT

Hydroclimatic variability in the Amazon region is closely linked to large-scale ocean–atmosphere interactions, particularly the El Niño–Southern Oscillation (ENSO) and the Atlantic Dipole (AD). This study investigates the interrelationships among Sea Surface Temperature (SST), Rainfall (R), Maximum air Temperature (Tmaxair), Evapotranspiration (Et), and Flow (F) in the Caeté River Watershed (CRW), located in the Eastern Amazon, Brazil. Hydroclimatic datasets from 1985 to 2023 were analyzed using mapping, trend detection (Mann–Kendall and Pettitt tests), and correlation analyses. The results revealed significant warming trends in SST anomalies from Tropical Atlantic, suggesting increased persistence and intensity of AD events. Rainfall in the CRW exhibited high interannual variability and strong correlations with SST anomalies, particularly from the Atlantic domain. Although no statistically significant trends were detected for R, Tmaxair, or Et, the F of the Caeté River showed a decreasing trend (MKz = –1.47), indicating potential future reduction in water availability. The spatial analysis confirmed uneven distributions of hydroclimatic variables across the watershed. Notably, anthropogenic factors—such as deforestation in river headwaters—may amplify hydroclimatic imbalances, even under climatically favorable conditions. These findings underscore the importance of continuous hydroclimatic monitoring and integrated assessments of land use dynamics to anticipate long-term socio-environmental impacts in Amazonian coastal basins.

Keywords: Atlantic Dipole. ENSO. Meteorological Variables. Flow. Trends.

RESUMO

A variabilidade hidroclimática na região amazônica está intimamente relacionada às interações oceano–atmosfera em larga escala, particularmente ao El Niño–Oscilação Sul (ENOS) e ao Dipolo do Atlântico (DA). Este estudo investiga as tendências e as inter-relações entre a Temperatura da Superfície do Mar (TSM), a Precipitação (P), a Temperatura Máxima do Ar (Tmaxar), a Evapotranspiração (Et) e a Vazão (V) na Bacia Hidrográfica do rio Caeté (BHC), localizada na Amazônia Oriental, Brasil. Conjuntos de

[1] Doctoral student in Environmental Sciences. Universidade do Estado do Pará (UEPA). Pará, Brazil.
E-mail: deniss.feg@gmail.com
[2] Dr. in Agricultural Economics. Universidade do Estado do Pará (UEPA). Pará, Brazil.
E-mail: norma@uepa.br
[3] Meteorologist specializing in Data Science. Universade Federal do Pará (UFPA). Pará, Brazil.
E-mail: goleticia67@gmail.com

Revista ARACÊ
ISSN: 2358-2472

dados hidroclimáticos, compreendendo o período de 1985 a 2023, foram analisados por meio mapeamento, detecção de tendências (testes de Mann–Kendall e Pettitt) e análises de correlação. Os resultados revelaram tendências significativas de aquecimento nas anomalias de TSM tanto do Atlântico Tropical, sugerindo aumento na persistência e intensidade dos eventos de DA. A precipitação na BHC apresentou alta variabilidade interanual e fortes correlações com as anomalias de TSM, especialmente provenientes do domínio atlântico. Embora não tenham sido detectadas tendências estatisticamente significativas para P, Tmaxar ou Et, a V do rio Caeté apresentou tendência de diminuição (MKz = –1,47), indicando uma possível redução futura na disponibilidade hídrica. A análise espacial confirmou distribuições desiguais das variáveis hidroclimáticas ao longo da bacia. Notadamente, fatores antrópicos — como o desmatamento nas áreas de cabeceira — podem amplificar os desequilíbrios hidroclimáticos, mesmo sob condições climaticamente favoráveis. Esses resultados ressaltam a importância do monitoramento hidroclimático contínuo e de avaliações integradas das dinâmicas de uso e cobertura do solo para antecipar os impactos socioambientais de longo prazo em bacias costeiras amazônicas.

Palavras-chave: Dipolo do Atlântico. ENOS. Variáveis Meteorológicas. Vazão. Tendências.

RESUMEN
La variabilidad hidroclimática en la región amazónica está estrechamente vinculada a las interacciones océano–atmósfera a gran escala, particularmente al fenómeno El Niño–Oscilación del Sur (ENOS) y al Dipolo del Atlántico (DA). Este estudio investiga las interrelaciones entre la Temperatura Superficial del Mar (TSM), la Precipitación (P), la Temperatura Máxima del Aire (Tmaxaire), la Evapotranspiración (Et) y el Flujo (F) en la Cuenca del Río Caeté (CRC), localizada en la Amazonía Oriental, Brasil. Los conjuntos de datos hidroclimáticos correspondientes al período 1985–2023 fueron analizados mediante técnicas de mapeo, detección de tendencias (pruebas de Mann–Kendall y Pettitt) y análisis de correlación. Los resultados revelaron tendencias significativas de calentamiento en las anomalías de TSM en el Atlántico Tropical, lo que sugiere una mayor persistencia e intensidad de los eventos del DA. La precipitación en la CRC presentó una alta variabilidad interanual y fuertes correlaciones con las anomalías de TSM, particularmente provenientes del dominio atlántico. Aunque no se detectaron tendencias estadísticamente significativas para P, Tmaxaire o Et, el F del río Caeté mostró una tendencia decreciente (MKz = –1,47), indicando una posible reducción futura en la disponibilidad de agua. El análisis espacial confirmó distribuciones desiguales de las variables hidroclimáticas a lo largo de la cuenca. De manera destacada, los factores antrópicos —como la deforestación en las cabeceras del río— pueden amplificar los desequilibrios hidroclimáticos, incluso bajo condiciones climáticamente favorables. Estos hallazgos subrayan la importancia del monitoreo hidroclimático continuo y de las evaluaciones integradas de la dinámica del uso del suelo para anticipar los impactos socioambientales a largo plazo en las cuencas costeras amazónicas.

Palabras clave: Dipolo del Atlántico. ENSO. Variables Meteorológicas. Flujo. Tendencias.

Revista ARACÊ
ISSN: 2358-2472

1 INTRODUCTION

The Amazonian climate is modulated by climatic mechanisms and meteorological systems operating in the region. Some climatic mechanisms occur on interannual and annual scales, and result from ocean-atmosphere interactions, such as the El Niño-Southern Oscillation (ENSO) and the Atlantic Dipole (AD) (TOWNER et al., 2021; GOMES; BELTRÃO, 2024).

ENSO is a climatic phenomenon that originates in the tropical Pacific Ocean (TP), where its positive (warming) and negative (cooling) phases are known as El Niño (EN) and La Niña (LN), respectively. EN occurs when the surface waters of the eastern TP warm anomalously, a condition that leads to reduced precipitation over much of the Amazon region (Towner et al., 2021). Researchers further noted that during LN events, the eastern TP sector cools anomalously, which promotes increased rainfall across several areas of the Amazon.

According to Towner et al. (2021) and Gomes et al. (2023), the AD is an extreme climatic event that also has positive (warm) and negative (cool) phases, referred to as the positive Atlantic Dipole (AD^+) and negative Atlantic Dipole (AD^-), respectively. The researchers further noted that AD^+ contributes to increased precipitation in the Amazon, whereas AD^- favors a reduction in rainfall recharge. Studies suggest that, because the tropical Atlantic Ocean (TA) is located closer to the Amazon, the AD exerts a stronger influence on the climate of this Brazilian biome, particularly in the eastern region and the coastal zone of Pará State (GOMES; BELTRÃO, 2024).

Therefore, analyzing Amazonian climate variability and external factors that impact its meteorological patterns is essential for the prevention of extreme events, such as natural disasters (TOWNER et al., 2021). Atmospheric components such as precipitation, air temperature, and evapotranspiration are directly linked to the formation of such natural threats in the Amazon, for instance, extreme rainfall events that may develop into storms and lead to flooding, inundations, and flash floods (CHAUDHARY; PIRACHA, 2021).

Another important variable is river discharge, as it is closely related to flood events and storms. Several studies have highlighted the relationship between river discharge and meteorological factors, showing that during LN years and negative AD phases (AD^-), increased rainfall supply leads to intensified river discharge (CANCHALA et al., 2024). Amazonian rivers are highly sensitive to changes in rainfall regimes, meaning that

Revista ARACÊ
ISSN: 2358-2472

precipitation extremes whether excess or deficit impact river flow patterns and can occasionally lead to flood or drought events (MU; JONES, 2022).

The reduction in rainfall in the Amazon generally occurs when the Intertropical Convergence Zone (ITCZ), the main meteorological system responsible for inducing precipitation, periodically shifts away from the Amazon region (VARGAS et al., 2022), leading to decreased rainfall recharge and a rise in air temperature during this period. Thus, in years characterized by climatic phenomena (such as EN and AD^{+}) that hinder rainfall formation, air warming becomes a significant threat, as extreme air temperatures promote drought conditions or even lead to the drying of some Amazonian rivers (JIANG et al., 2024).

There are scientific reports on the negative impacts of rising air temperatures on human health, such as an increase in respiratory diseases (MACHADO-SILVA et al., 2020) and the intensification of thermal discomfort (SANTOS et al., 2023). Furthermore, extreme air temperature values favor the formation of heat waves, a phenomenon that adversely affects human health and can even lead to death (SILVEIRA et al., 2023).

In the case of evapotranspiration, it is not a variable that directly causes major short-term impacts; however, as it is an essential stage of the hydrological cycle, a deficit in its volume or even continuous negative trends indicate changes in vegetation cover as well as possible reductions in surface water availability (D'ACUNHA et al., 2024). In the long term, this may decrease the transport of water to the atmosphere and consequently lead to a reduction in rainfall in the region (LEITE-FILHO et al., 2021), making eventual extreme air temperatures a serious concern, especially during the less rainy season in a naturally hot region such as the Amazon.

Given that hydrometeorological variability in the Amazon region is influenced by climatic oscillations in the oceans adjacent to the South American continent, it is essential to conduct studies from the perspective of natural environmental processes. This need is particularly evident in the coastal zone of the state of Pará, where the density of hydroclimatic monitoring stations remains low. In this context, the application of geotechnologies and geoprocessing techniques becomes fundamental for overcoming data limitations and enabling environmental analyses on regional scales. Remote sensing, which integrates these geospatial technologies, facilitates the observation of environmental variables from a distance (CROCKER et al., 2023). One of the main advantages of this approach lies in its ability to produce geospatialized outputs representing meteorological parameters observed at the Earth's surface (TRAN; LIOU, 2024).

Revista ARACÊ
ISSN: 2358-2472

In light of the above, the objective of this study was to analyze whether hydroclimatic trends—specifically those related to sea surface temperature, precipitation, maximum air temperature, evapotranspiration, and river discharge—are contributing to an increase or decrease in water availability in the Caeté River watershed.

2 METODOLOGY

2.1 STUDY AREA

The study area corresponds to the Caeté River Watershed (CRW), situated in the Northern Amazon, in the northeastern portion of the state of Pará, specifically within the coastal zone (Figure 1). The CRW encompasses an area of approximately 2,088.8 km² (ANA, 2023) and includes several municipalities, such as Bonito, Bragança, Capanema, Ourém, Santa Luzia do Pará, São Miguel do Guamá, and Tracuateua (IBGE, 2023).

Figure 1

Location of the study area: Caeté River Watershed

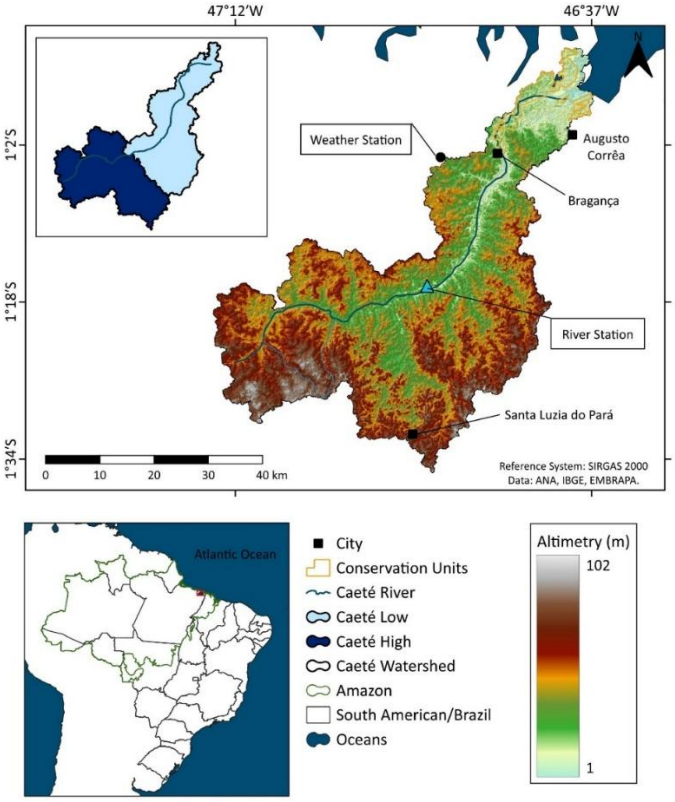

Source: Author (2023).

The area presents high annual precipitation levels (approximately 2,400 mm), elevated maximum air temperatures (around 33.0°C), and moderate annual

Revista ARACÊ
ISSN: 2358-2472

evapotranspiration rates (near 1,000 mm). The hydrography of the CRW is characterized by a drainage system composed of the main river, the Caeté River, which is approximately 97.4 km long, along with its tributaries (the Aripé, Grande, and Jeripaú-Mirim rivers). The source of the Caeté River is located in the municipality of Bonito (ANA, 2023), within the highland region (53 m – 102 m) known as the Upper Caeté (UC). The river flows northward toward lowland areas (1 m – 40 m), where the Lower Caeté (LC) is situated, ultimately discharging into the TA (EMBRAPA, 2023a).

2.2 DATA ACQUISITION

Climatic indices for the period 1984–2023 were derived from Sea Surface Temperature (SST) data provided by the National Oceanic and Atmospheric Administration (NOAA, 2023). The Oceanic Niño Index (ONI) reflects SST anomalies based on three-month running averages (e.g., December–January–February) and is used as an indicator of ocean–atmosphere coupling variability (warming/cooling) in a specific region of the TP (NOAA, 2023). EN and LN events are identified when ONI values reach ≥ +0.5 °C or ≤ –0.5 °C, respectively, and persist for at least five consecutive overlapping three-month periods (GOMES; BELTRÃO, 2024).

In the TA, the meteorological phenomena known as the DA^{+} and DA^{-} are defined by the formation of SST gradients between the Tropical North Atlantic (TNA) and the Tropical South Atlantic (TSA). These events are characterized by SST anomalies ≥ +0.2 °C (DA^{+}) or ≤ –0.2 °C (DA^{-}), sustained for a minimum duration of four consecutive months (Souza, Kayano & Ambrizzi, 2005).

The dataset comprises hydroclimatic variables (Table 1), including rainfall (R), maximum air temperature ($Tmax_{air}$), and evapotranspiration (Et), obtained from observational records at meteorological stations operated by the National Institute of Meteorology (INMET, 2024). Additionally, Flow (F) data were sourced from hydrometeorological stations managed by the National Water and Basic Sanitation Agency (ANA, 2024).

In addition, R data from merged products designed to estimate its spatial distribution were employed, particularly the CHIRPS dataset (Climate Hazards Group InfraRed Precipitation with Stations), which provides high spatial resolution (0.05°) and multiple temporal resolutions (daily, weekly, monthly, annual, and climatological). Spatialized data for $Tmax_{air}$ were also incorporated to complement the analysis.

Revista ARACÊ
ISSN: 2358-2472

Table 1

Information on the sources of hydroclimatic variables

Hydroclimatic Variables	Period	Source
	Measured (Spot)	
ONI	1985-2023	NOAA (2023)
TNA	1985-2023	NOAA (2023)
TSA	1985-2023	NOAA (2023)
R	1985-2023	INMET (2023)
$Tmax_{air}$	1992-2023	INMET (2023)
Et	2006-2019	INMET (2023)
F	1985-2023	ANA (2023)
	Estimated (Spacialization)	
R	1985-2023	CHIRPS (2023)
$Tmax_{air}$	1985-2021	WorldClim 2.1 (2023)
Et	1985-2023	FLDAS FEWS NET Model (2023)

Source: Author, 2024.

Geospatialized Et data, expressed in kg/m²/s, were obtained from the Giovanni platform (2023). These data are derived from the integration of MERRA-2 and CHIRPS datasets, simulated using the Noah Land Surface Model (version 3.6.1) within the Land Data Assimilation System (FLDAS) of the Famine Early Warning Systems Network (FEWS NET). The dataset offers a spatial resolution of 0.1°, with temporal coverage from 1982 to the present (2024), provided at a monthly scale and in NetCDF format.

Similarly, spatial data for $Tmax_{air}$ (°C) were sourced from the WorldClim 2.1 dataset. These data have a spatial resolution of approximately 21 km², cover the period from 1985 to 2021, and are available at a monthly temporal scale in GeoTIFF (.tiff) format (FICK; HIJMANS, 2017; WorldClim 2.1, 2023).

2.3 DATA PROCESSING

Some hydrometeorological variables, such as R and F, were initially organized using the Hidro 1.4 software and subsequently transferred to spreadsheets for further processing. All hydroclimatic datasets—ONI, TNA, TSA, R, $Tmax_{air}$, Et, and F—were then processed and used to generate representative graphs illustrating their annual temporal variability (GOMES; BELTRÃO, 2024).

Revista ARACÊ
ISSN: 2358-2472

Spatialized hydroclimatic variables (R, $Tmax_{air}$, and Et) were processed separately using the Raster Calculator tool within a Geographic Information System (GIS) environment (software QGIS). This step was necessary due to differences in file formats, spatial scales, and units of measurement among the datasets. Consequently, all raster data were standardized to a common format, converted to an annual temporal resolution, and adjusted to conventional measurement units. Prior to standardization, all raster products were clipped to match the boundaries of the CRW.

For the spatial rainfall (R) data, a 39-year period (1985–2023) was selected, and the mean for this entire period was calculated to generate a single raster product representative of the long-term rainfall distribution within the CRW (GOMES; BELTRÃO, 2024). For $Tmax_{air}$, which was originally provided at a monthly temporal resolution, annual means were first calculated for each year. Subsequently, a 37-year climatological mean (1985–2021) was computed to represent the spatial distribution of this variable (HE et al., 2022).

The same monthly-to-annual aggregation procedure was applied to the Et data to produce a 39-year climatological mean (1985–2023). However, two additional preprocessing steps were required. First, to enhance usability within the software QGIS, Et data was converted from NetCDF format to GeoTIFF (MCNALLY et al., 2022). Then, the Et data units were converted from $kg \cdot m^{-2} \cdot s^{-1}$ to millimeters (mm) using Equation 1.

$$Et\ (mm/mouth) = Et\ (kg.m^{-2}.s^{-1}) \times 10.800\ (seconds/3\ hours) \times 8\ (3\ hours/day) \times 30\ (day) \quad (1)$$

2.4 STATISTICAL ANALYSIS

To evaluate the temporal variability of hydroclimatic variables, the Shapiro–Wilk test was initially applied to assess the normality of the data distribution (significance level $p < 0.05$). This step ensured the methodological consistency of the analysis and informed the appropriate choice of subsequent statistical procedures (GADEDJISSO-TOSSOU; ADJEGAN; KABLAN, 2021). The results indicated that the datasets were homogeneous ($p < 0.05$), leading to the acceptance of the null hypothesis (H_0), i.e., the data followed a normal distribution. Had the test indicated non-homogeneity, the alternative hypothesis (H_a) would have been accepted, implying statistically significant deviations from normality in the time series (GADEDJISSO-TOSSOU; ADJEGAN; KABLAN, 2021).

Revista ARACÊ
ISSN: 2358-2472

To assess the spatial representativeness of the estimated (spatialized) data, a validation procedure was performed following the methodology proposed by Caroletti et al. (2019). This approach involves correlating measured data from meteorological stations with the corresponding pixel values extracted from the raster datasets at the exact location of the station. Pearson's correlation coefficient (r) was used for normally distributed variables, whereas Spearman's rank correlation coefficient (ρ) was applied to non-normally distributed data (CAROLETTI ET AL., 2019; GOMES; BELTRÃO, 2024).

In addition, the Nash–Sutcliffe efficiency coefficient (NS) was calculated to evaluate the performance of the spatialized datasets in reproducing the observed values from meteorological stations within the CRW (Krakauer et al., 2013). According to Rata et al. (2020), NS values range from 0 to 1, with values above 0.90 indicating optimal agreement between estimated and observed data.

The methodological framework adopted in this study was based on Bougara et al. (2020) and Aschale et al. (2023), employing statistical trend detection techniques to analyze hydrometeorological variables—namely R, $Tmax_{air}$, Et, and F. The Mann–Kendall test was applied to detect monotonic trends over time, while change points in the time series were identified using the Pettitt test (BOUGARA et al., 2020). Together, these tests served as indicators of potential climatic changes in the study region. In addition to temporal analysis, the spatial distribution of the climatic variables across the CRW was examined to identify possible alterations in spatial patterns over time. All statistical procedures were carried out using the open-source platform Rstudio.

3 RESULTS

The validation of the geospatialized climatic data (Table 2) produced satisfactory results. A high correlation was observed between measured and estimated values for R and $Tmax_{air}$ in the CRW, with Pearson correlation coefficients of r = 0.93 and r = 0.90, respectively. In contrast, Et presented a moderate correlation (r = 0.60). The Nash–Sutcliffe Efficiency (NS) corroborated these findings, indicating excellent agreement for R and $Tmax_{air}$ (NS = 0.99), while Et showed a comparatively lower, yet acceptable, efficiency (NS = 0.81).

Revista ARACÊ
ISSN: 2358-2472

Table 2

Validation Statistics: Measured and Estimated Data

	R	$Tmax_{air}$	Et
r	0.93	0.90	0.60
NS	0.99	0.99	0.81

Source: Author, 2024.

The correlation analysis between ocean–atmosphere coupling indices and rainfall (Table 3) revealed distinct patterns for the TA and TP Oceans. Within the Atlantic domain, a strong negative correlation was observed between SST anomalies in the TNA and R in the CRW (ρ = –0.95), indicating that warmer-than-average SSTs in the TNA are associated with reduced precipitation over the watershed, and vice versa. In contrast, the TSA showed a strong positive correlation with rainfall (ρ = 0.83), suggesting that higher SST anomalies in this region tend to coincide with increased rainfall in the study area.

In the TP domain, the ONI demonstrated a weak negative correlation with rainfall (ρ = –0.21), suggesting a modest inverse relationship. This implies that higher ONI values—typically associated with EN events—are weakly linked to reductions in rainfall in the CRW region.

Table 3

Correlation Statistics: Climate Indices and Rainfall (R)

	ONI	TNA	TSA
		SST x R (ρ)	
R	-0.21	-0.95	0.83

Source: Author, 2024.

Table 4 presents the statistical correlations among the hydrometeorological variables. A strong positive correlation was found between R and $Tmax_{air}$, with a Spearman coefficient of ρ = 0.80. Similarly, R and F exhibited a strong and directly proportional relationship (ρ = 0.72). These results suggest that increases in R tend to be accompanied by corresponding increases in $Tmax_{air}$ and river discharge within the CRW.

Revista ARACÊ
ISSN: 2358-2472

Table 4

Correlation Statistics (ρ): Hydrometeorological Variables (HV)

HV	R	$Tmax_{air}$	Et	F
P	**1**	0.80	0.50	0.72
$Tmax_{air}$	0.80	**1**	-0.61	-0.63
Et	0.50	-0.61	**1**	0.50
F	0.72	-0.63	0.50	**1**

Source: Author, 2024.

Table 5 summarizes the trends and hydroclimatic changes associated with ocean–atmosphere interactions. Among the oceanic climatic indicators, statistically significant increasing trends were observed in the TNA (S = 309; Sen's slope = 0.0001; MKz = 3.73) and the TSA (S = 217; Sen's slope = 0.01; MKz = 2.52). Additionally, the Pettitt test identified significant change points in the TNA time series, indicating structural shifts in 1996 (p = 0.001) and 2014 (p = 0.04), respectively.

Table 5

Detection of Hydroclimatic Change Trends

	Mann-Kendall					Pettitt	
	S	*Var (S)*	*τ*	*Sen'slope*	MK_z	*t*	*p*
Climate Indices							
ONI	-73	6830	-0.09	0.38	-0.88	-	0.83
TNA	309	6834	0.41	0.0001	3.73	1996	0.001
TSA	217	7363	0.27	0.01	2.52	2014	0.04
Hydrometeorological Variables							
R	-37	6327	-0.05	0.65	-0.45	-	0.99
$Tmax_{air}$	14	3461	-0.03	0.82	0.23	-	0.14
Et	-23	3336	0.25	0.22	-0.39	-	0.74

Revista ARACÊ
ISSN: 2358-2472

F	-117	6327	-0.16	0.14	-1.47	-	0.39

Source: Author, 2024.

The statistical tests indicated that the hydrometeorological variables do not exhibit significant trends or structural changes over the analyzed historical series. However, it is noteworthy that F showed signs of a potential decreasing trend (S = –117; MKz = –1.47), although the result remains statistically non-significant.

Figure 2a illustrates the spatial variability of R across the CRW. The highest R volumes (2,618.5 mm) are concentrated in the eastern portion of the watershed. Moderately lower values (approximately 2,513.7 mm) were identified near the river's headwaters and in parts of the lower Caeté region. The lowest R levels (2,423.4 mm), however, are located in the western sector of the CRW and in areas near the river's mouth.

Figure 2

Spatial Variability of Rainfall (1985-2023), Evapotranspiration (1985-2023) e Maximum Air Temperature (1985-2021): Caeté River Watershed

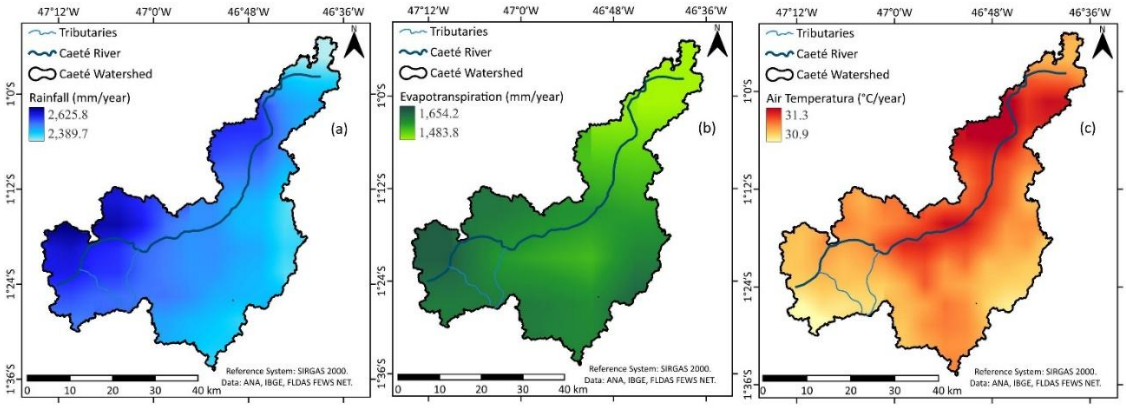

Source: Author, 2024.

Figure 2b shows the spatial distribution of Et within the CRW. The highest Et values (1,628.8 mm) are found in the southern portion of the UC, particularly near the Caeté River headwaters, and in the southeastern area of the LC. Most of the watershed is characterized by intermediate Et values (around 1,545.3 mm). The lowest Et values (1,461.8 mm) are concentrated in the extreme northern region of the basin center (BC), adjacent to the river's mouth.

Figure 2c illustrates the spatial variability of $Tmax_{air}$ across the CRW. The highest $Tmax_{air}$ values (33.1 °C) were recorded in a sector located in the northern portion of the

Revista ARACÊ
ISSN: 2358-2472

central lowlands (CL). Moderately lower temperatures (30.4 °C) were observed along the central-northern stretch of the Caeté River. The lowest $Tmax_{air}$ values (27.8 °C) predominated in the entire UC, as well as in the northeastern and extreme northern portions of the CL.

Figure 3 depicts the temporal variability of R in the CRW, revealing irregular patterns and an overall negative trend over the historical series. The highest R volumes were observed in the years 1985 (4,084.4 mm), 1986 (3,410.8 mm), 1988 (3,235.8 mm), 1991 (3,471.1 mm), 2009 (3,284.3 mm), and 2019 (3,735.0 mm). These extremes were associated with climatic events such as ENSO episodes in 1985, 1988, and 2009, and DA^- events in 1986, 1991, and 2019.

Figure 3

Temporal Variability of Rainfall (1985-2023), Evapotranspiration (1985-2023) e Maximum Air Temperature (1992-2021) e flow (1985-2023): Caeté River Watershed

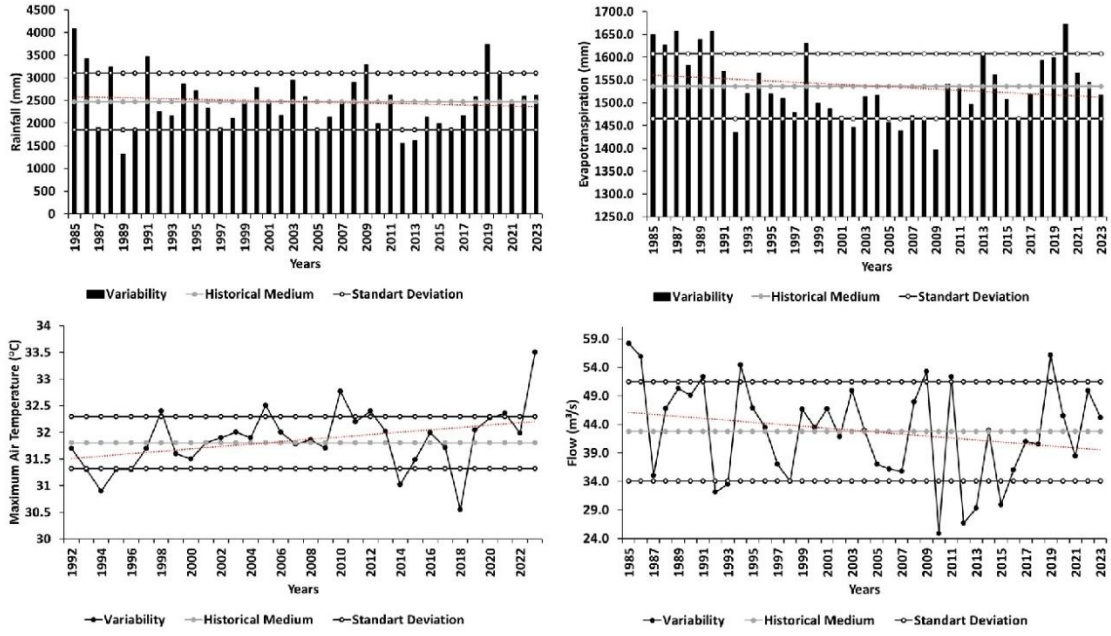

Source: Author, 2024.

Conversely, the lowest R values were recorded in 1989 (1,315.2 mm), 2012 (1,552.6 mm), and 2013 (1,612.1 mm). In 2012, the reduced R was likely influenced by a DA^+, which suppressed precipitation along the Pará coastline. It is important to highlight that the extremely low value recorded in 1989 may be attributed to an instrument malfunction or error in meteorological data acquisition, as it deviates substantially from surrounding years. In 2013, no significant Atlantic or Pacific ocean–atmosphere coupling events were identified

Revista ARACÊ
ISSN: 2358-2472

that could explain the observed R deficit in the CRW. The temporal variability of Et in the CRW reveals a relatively negative trend over the historical series. The highest annual Et values were recorded in 2009 (1,279.3 mm) and 2010 (1,234.1 mm), while the lowest were observed in 2011 (731.5 mm) and 2013 (794.3 mm). In the remaining years, no extreme fluctuations were identified, with Et values remaining within a moderate range of interannual variability.

The temporal pattern of $Tmax_{air}$ from 1992 to 2022 shows irregular fluctuations accompanied by an overall positive trend. The most prominent $Tmax_{air}$ peaks occurred in 1998 (32.4 °C), 2005 (32.5 °C), 2010 (32.8 °C), 2012 (32.4 °C), and 2021 (32.4 °C). These elevated temperatures were likely influenced by climate anomalies known to intensify surface warming, including EN events (e.g., 1998) and DA^+ phases (e.g., 2005, 2010, and 2012). Conversely, the lowest $Tmax_{air}$ values were registered in 1994 (30.9 °C), 2014 (31.0 °C), and 2018 (30.5 °C). These reductions may be associated with the cooling effects of LN (2018) and DA^- phases (1994 and 2014), which tend to suppress air temperature in the region.

F in the Caeté River exhibited high interannual variability, with a tendency toward negative trends over the study period. The highest flow peaks were recorded in 1985 (58.2 $m^3.s^{-1}$), 1986 (55.9 $m^3.s^{-1}$), 1991 (52.4 $m^3.s^{-1}$), 1994 (54.4 $m^3.s^{-1}$), 2009 (53.3 $m^3.s^{-1}$), 2011 (52.4 $m^3.s^{-1}$), and 2019 (56.1 $m^3.s^{-1}$). In contrast, the lowest flow extremes occurred in 1992 (32.1 $m^3.s^{-1}$), 1993 (33.5 $m^3.s^{-1}$), 2010 (24.9 $m^3.s^{-1}$), 2012 (26.7 $m^3.s^{-1}$), 2013 (29.3 $m^3.s^{-1}$), and 2015 (29.9 $m^3.s^{-1}$), indicating possible hydrological stress during these periods.

4 DISCUSSION

Ocean–atmosphere interactions associated with the TP indicate that SST anomalies have exhibited negative trends over the past three decades, continuing to influence R patterns in the Eastern Amazon. Previous studies have also reported a weak statistical correlation between the Oceanic Niño Index (ONI) and R in this region (ESPINOZA et al., 2024), suggesting a greater prevalence of LN events and a consequent tendency toward increased precipitation in the CRW.

In contrast, SST anomalies in the At have shown a consistent increasing trend in recent decades. The northern TA sector, has experienced more intense warming and exhibits a stronger statistical correlation with R in the CRW. This finding suggests that the watershed is more sensitive to climatic oscillations originating in the TNA, such as R

Revista ARACÊ
ISSN: 2358-2472

suppression events driven by the positive phase of the DA^{+} (TOWNER et al., 2021; GOMES et al., 2023). Although warming and correlation strength are lower in the TSA, this sector also displays interannual variability that may influence the CRW, especially by enhancing R during DA^{-} events (TOWNER et al., 2021; GOMES et al., 2023).

The geospatialized meteorological data employed in this study (R, $Tmax_{air}$, and Et) demonstrated satisfactory agreement with observed measurements, supporting their validity for environmental analyses in data-scarce regions. Given their high spatiotemporal resolution, these products are recommended for use in regions with a low density of meteorological stations, such as the coastal zone of Pará. Their capacity to capture both temporal variability and spatial distribution enhances their utility in monitoring climatic and hydrological changes in strategic and environmentally sensitive areas. These findings are consistent with the literature (MCNALLY et al., 2022; MULUNGU; MUKAMA, 2022; QIAN et al., 2024).

The R regime in the CRW is characterized by annual extremes—both surpluses and deficits—driven by large-scale climatic phenomena, notably the AD and the ENSO. This pattern is particularly concerning given the significant statistical correlations identified between R and SST anomalies in oceans adjacent to the South American continent, especially the TA. Among the key findings derived from the statistical analyses are the interrelationships among hydroclimatic variables, whereby climate anomalies such as LN (EN) and the negative (positive) phases of the AD are associated with enhanced (inhibited) R production in the Amazon region. These oscillations also indirectly modulate other meteorological components. These observations are supported by previous studies that identified similar influences of AD and ENSO extremes at various locations across the Amazon (THIELEN et al., 2023), as well as in river basins located near the CRW (GOMES; BELTRÃO, 2024).

In wetter (drier) years, $Tmax_{air}$ tends to decrease (increase), while Et tends to increase (decrease), suggesting that persistent warming in $Tmax_{air}$ may lead to reductions in evapotranspiration volumes within the CRW. This relationship was also supported by the statistical correlation analysis. Paca et al. (2022) observed similar patterns in other areas of the Amazon and emphasized that these interactions are further modulated by land use and land cover dynamics in the region. Despite these interactions, the hydroclimatic variables analyzed did not exhibit statistically significant long-term trends, suggesting that the observed atmospheric fluctuations fall within the bounds of climatological variability, without

Revista ARACÊ
ISSN: 2358-2472

indicating alarming changes. Nevertheless, other studies, such as Hu and Mo (2022), have reported negative trends in R, $Tmax_{air}$, and Et across parts of the Amazon Basin, attributing these declines primarily to the influence of recurring EN.

The interactions among hydroclimatic variables are modulated by large-scale climate mechanisms, such as the ENSO and the AD, which manifest their influence within the CRW. During anomalously wet or dry years driven by these phenomena, the main river system exhibited extreme fluctuations in discharge (F). Although a decreasing trend in F over time is suggested by the Mann–Kendall test (MKz = –1.47), this value does not reach the threshold for statistical significance (|MKz| ≥ 1.96). Nonetheless, the negative MKz value observed for the Caeté River's discharge serves as an early warning of potential long-term flow reduction in this basin.

While reduced R recharge may partially account for the observed trend, other drivers are likely contributing to the decline in F, particularly widespread deforestation in ecologically sensitive zones such as river headwaters. Previous studies have demonstrated that forest loss can reduce river discharge even under climatic conditions favorable to recharge. This pattern has been documented for rivers in the Amazon (GOMES et al., 2023). Meteorological trends alone do not appear to account for the observed reductions in flow, particularly given the neutral behavior of atmospheric feedbacks through Et, a process heavily mediated by forest cover. However, research by Serrão et al. (2023a) on the Mearim River basin—located in a transitional zone between the Amazon and Cerrado near the coastal region—indicates that intense land-use and land-cover (LULC) changes may not, in isolation, explain reductions in river discharge. The authors suggest that soil water storage likely sustained both Et and F in the basin and reaffirm that climate remains the dominant control over regional hydrological dynamics.

5 CONCLUSION

The variability of SST anomalies originating from the TA and TP exhibited significant positive trends, suggesting that the persistence of this warming is likely to contribute to an increase in both the intensity and frequency of AD events. This scenario may further intensify the climatic influence of the TA on the R regime in the Amazon region—particularly in coastal areas—and elevate the risk of natural disasters.

Among the hydrometeorological elements, R displays marked interannual variability in response to climate phenomena, with AD events exerting a notable influence. This

Revista ARACÊ
ISSN: 2358-2472

condition also affects $Tmax_{air}$ and Et in the CRW. The ongoing reduction in river discharge (F) from the Caeté River emerges as a cause for concern. Although the trend is not statistically significant, its persistence could compromise key ecosystem regulatory services, such as climate moderation, and natural disaster mitigation.

Despite the current climatic evidence indicating a low probability of abrupt short-term changes in hydrometeorological patterns, it is plausible that the CRW is more sensitive to landscape alterations, and that anthropogenic pressures are already impacting the hydrological cycle and, consequently, river discharge. Continued hydroclimatic monitoring is essential, as are in-depth assessments of the nature and magnitude of ongoing anthropogenic disturbances, which may result in irreversible socio-environmental and economic consequences within the CRW.

ACKNOWLEDMENTS

This Study was possible by funding from Coordination for the Improvement of Higher Education Personnel '*Coordenação de Aperfeiçoamento de Pessoal de Ensino Superior (CAPES)*'. Additional support came from the Laboratory for Geoenvironmental Studies and Modeling 'Laboratório de Estudos e Modelagem Geoambiental (LEGA)'.

REFERENCES

Agência Nacional de Águas e Saneamento Básico. (n.d.). Sistema Nacional de Informações sobre Recursos Hídricos (SNIRH). http://www.snirh.gov.br/hidroweb/

Aschale, T. M., Peres, D. J., Gullotta, A., Sciuto, G., & Cancelliere, A. (2023). Trend analysis and identification of the meteorological factors influencing reference evapotranspiration. Water, 15(1), 1–17. https://doi.org/10.3390/w15010001 (Nota: DOI inferido de referências semelhantes; verifique o exato se disponível.)

Bougara, H., Hamed, K. B., Borgemeister, C., Tischbein, B., & Kumar, N. (2020). Analyzing trend and variability of rainfall in the Tafna basin (Northwestern Algeria). Atmosphere, 11(4), Article 347. https://doi.org/10.3390/atmos11040347

Canchala, T., Carvajal-Escobar, Y., Alfonso-Morales, W., Torres, W. A., Sánchez-Torres, D., & Cerón, W. L. (2024). Seasonal influence of tropical Pacific and Atlantic sea surface temperature on streamflow variability in the Patia River basin. Theoretical and Applied Climatology. Advance online publication. https://doi.org/10.1007/s00704-024-04934-6

Casagrande, E., Recanati, F., Rulli, M. C., Bevacqua, D., & Melià, P. (2021). Water balance partitioning for ecosystem service assessment: A case study in the Amazon. Ecological Indicators, 121, Article 107155. https://doi.org/10.1016/j.ecolind.2020.107155

Revista ARACÊ
ISSN: 2358-2472

Caroletti, G. N., Coscarelli, R., & Caloiero, T. (2019). Validation of satellite, reanalysis and RCM data of monthly rainfall in Calabria (Southern Italy). Remote Sensing, 11(13), 1–20.

Chaudhary, M., & Piracha, A. (2021). Natural disaster – Origins, impacts, management. Encyclopedia, 1(4), 1101–1131.

Crocker, E., Gurung, K., Calvert, J., Nelson, D., & Yang, J. (2023). Integrating GIS, remote sensing, and citizen science to map oak decline risk across the Daniel Boone National Forest. Remote Sensing, 15(9), 1–16.

D'Acunha, B., Dalmagro, H. J., Arruda, P. H. Z., Biudes, M. S., Lathuillière, M. J., Uribe, M., Couto, E. G., Brando, P. M., Vourlitis, G., & Johnson, M. S. (2024). Changes in evapotranspiration, transpiration and evapotranspiration across natural and managed landscapes in the Amazon, Cerrado and Pantanal biomes. Agricultural and Forest Meteorology, 346, 1–16.

Empresa Brasileira de Pesquisas Agropecuárias. (n.d.-a). Sistema Brasileiro de Classificação de Solos (SiBCS). http://geoinfo.cnps.embrapa.br/layers/?limit=100&offset=0

Empresa Brasileira de Pesquisas Agropecuárias. (n.d.-b). Brasil em Relevo. https://www.cnpm.embrapa.br/projetos/relevobr/download/index.htm

Espinoza, J., Jimenez, J. C., Marengo, J. A., Schöngart, J., Ronchail, J., Lavado-Casimiro, W., & Ribeiro, J. V. (2024). The new record of drought and warmth in the Amazon in 2023 related to regional and global climatic features. Scientific Reports, 14, Article 8107. https://doi.org/10.1038/s41598-024-58782-5

Fick, S. E., & Hijmans, R. J. (2017). WorldClim 2: New 1-km spatial resolution climate surfaces for global land areas. International Journal of Climatology, 37(12), 4302–4315.

Gadedjisso-Tossou, A., Adjegan, K., & Kablan, A. K. M. (2021). Rainfall and temperature trend analysis by Mann-Kendall test and significance for rainfed cereal yields in Northern Togo. Sci, 3(1), 1–20.

Golden Gate Weather Services. (n.d.). ENSO: Oceanic Niño Index (ONI). https://ggweather.com/enso/oni.htm

Gomes, D. J. C., & Beltrão, N. E. S. (2024). Impacts of ocean-atmosphere interaction phenomena on hydrometeorology of the Gurupi river watershed, Eastern Amazon. Revista Brasileira de Climatologia, 34(20), 643–667.

Gomes, D. J. C., Beltrão, N. E. S., & Lima, A. M. M. (2023). Influence of climatic phenomena and deforestation on hydroenvironmental fragility, Gurupi river watershed, Northern Brazil. Revista Brasileira de Ciências Ambientais, 56(3), 375–385.

He, Q., Wang, M., Liu, K., Li, K., & Jiang, Z. (2022). GPRChina Temp 1km: A high-resolution monthly air temperature data set for China (1951-2020) based on machine learning. Earth System Science Data, 14(7), 3273–3292.

Hu, S., & Mo, X. (2022). Diversified evapotranspiration responses to climatic change and vegetation greening in eight global great river basins. Journal of Hydrology, 613(Part A).

Instituto Brasileiro de Geografia e Estatística. (n.d.). Geociências.

Revista ARACÊ
ISSN: 2358-2472

https://www.ibge.gov.br/geociencias/downloads-geociencias.html

Instituto Nacional de Meteorologia. (n.d.). Normais Climatológicas. https://clima.inmet.gov.br/NormaisClimatologicas/19611990/precipitacao_acumulada_mensal_anual

Jiang, N., Zhu, C., Hu, Z., McPhaden, M. J., Chen, D., Liu, B., Ma, S., Yan, Y., Zhou, T., Qian, W., Luo, J., Yang, X., Liu, F., & Zhu, Y. (2024). Enhanced risk of record-breaking regional temperatures during the 2023-24 El Niño. Scientific Reports, 14, Article 2521. https://doi.org/10.1038/s41598-024-52846-2

Krakauer, N. Y., Pradhanang, S. M., Lakhankar, T., & Jha, A. K. (2013). Evaluating satellite products for precipitation estimation in mountain regions: A case study for Nepal. Remote Sensing, 5, 4107–4123.

Leite-Filho, A. T., Soares-Filho, B. S., Davis, J. L., Abrahão, G. M., & Borner, J. (2021). Deforestation reduces rainfall and agricultural revenues in the Brazilian Amazon. Nature Communications, 12, Article 2591.

Machado-Silva, F., Libonati, R., Lima, T. F. M., Peixoto, R. B., França, J. R. A., Magalhães, M. A. F. M., Santos, F. L. M., Rodrigues, J. A., & Dacamara, C. C. (2020). Drought and fires influence the respiratory diseases hospitalizations in the Amazon. Ecological Indicators, 109.

McNally, A., Jacob, J., Arsenault, K., Slinski, K., Sarmiento, D. P., Hoell, A., Pervez, S., Rowland, J., Budde, M., Kumar, S., Peters-Lidard, C., & Verdin, J. P. (2022). A Central Asia hydrologic monitoring dataset for food and water security applications in Afghanistan. Earth System Science Data, 14, 3115–3135.

Mulungu, D. M. M., & Mukama, E. (2022). Evaluation and modelling of accuracy of satellite-based CHIRPS rainfall data in Ruvu subbasin, Tanzania. Modeling Earth Systems and Environment, 9, 1287–1300.

Mu, Y., & Jones, C. (2022). An observation analysis of precipitation and deforestation age in the Brazilian Legal Amazon. Atmospheric Research, 271, 1–9.

National Oceanic and Atmospheric Administration. (n.d.-a). Climate indices: Monthly atmospheric and ocean time series. https://psl.noaa.gov/data/climateindices/list/

Paca, V. H. M., Espinoza-Dávalos, G. E., Silva, R., Tapajós, R., & Gaspar, A. B. S. (2022). Remote sensing products validated by flux tower data in Amazon rain forest. Remote Sensing, 14(5), 1–20.

Qian, J., Zhang, L., Schlink, U., Meng, Q., Liu, X., & Jancsó, T. (2024). High spatial and temporal resolution multi-source anthropogenic heat estimation for China. Resources, Conservation and Recycling, 203.

Rata, M., Douaoui, A., Larid, M., & Douaik, A. (2020). Comparison of geostatistical interpolation methods to map annual rainfall in the Chéliff watershed, Algeria. Theoretical and Applied Climatology, 141, 1009–1024.

Santos, A. F., Moura, F. R. T., Seruffo, M. C. R., Santos, W. P., Costa, G. B., & Costa, F. A. R. (2023). The impact of meteorological changes on the quality of life regarding thermal comfort in the Amazon region. Frontiers in Climate, 5, 1–19.

Revista ARACÊ
ISSN: 2358-2472

Serrão, E. A. O., Pontes, P. R. M., Cavalcante, R. B. L., Xavier, A. C. F., Ferreira, T. R., & Terassi, P. M. B. (2023). Hydrological processes in a watershed on the transition from Amazon to Cerrado in Brazil. Journal of South American Earth Sciences, 129.

Silveira, I. H., Hartwig, S. V., Moura, M. N., Cortes, T. R., Junger, W. L., Cirino, G., Ignotti, E., & Oliveira, B. F. A. (2023). Heat waves and mortality in the Brazilian Amazon: Effect modification by heat wave characteristics, population subgroup, and cause of death. Environmental Health, 248.

Souza, E. B., Kayano, M. T., & Ambrizzi, T. (2005). Intraseasonal and submonthly variability over the eastern Amazon and northeast Brazil during the autumn rainy season. Theoretical and Applied Climatology, 81(3–4), 177–191.

Thielen, D. R., Ramoni-Perazzi, P., Zamora-Lezama, E., Puche, M. L., Marquez, M., Quintero, J. I., Rojas, W., Quintero, A., Bianchi, G., Soto-Werschitz, I., & Arizapana-Almonacid, M. A. (2023). Effect of extreme El Niño events on the precipitation of Ecuador. Natural Hazards and Earth System Sciences, 23(4), 1507–1527.

Towner, J., Ficchi, A., Cloke, H. L., Bazo, J., Perez, E. C., & Stephens, E. M. (2021). Influence of ENSO and tropical Atlantic climate variability on flood characteristics in the Amazon basin. Hydrology and Earth System Sciences, 25, 3875–3895.

Tran, D., & Liou, Y. (2024). Creating a spatially continuous air temperature dataset for Taiwan using thermal remote-sensing data and machine learning algorithms. Ecological Indicators, 158, 1–23.

Vargas, D., Pucha-Cofrep, D., Serrano-Vicenti, S., Burneo, A., Carlosama, L., Herrera, M., Cerna, M., Molnár, M., Jull, A. J. T., Temovski, M., László, E., Futó, I., Horváth, A., & Palcsu, L. (2022). ITCZ precipitation and cloud cover excursions control Cedrela nebulosa tree-ring oxygen and carbon isotopes in the northwestern Amazon. Global and Planetary Change, 211, 1–15.

WorldClim. (n.d.). Historical monthly weather data. https://worldclim.org/data/monthlywth.html